Article

Experimental Diagnosis of Broken Rotor Bar Faults in Induction Motors at Low Slip via Hilbert Envelope and Optimized Subtractive Clustering Adaptive Neuro-Fuzzy Inference System

Seif Eddine Chehaidia [1], **Hakima Cherif** [2], **Musfer Alraddadi** [3], **Mohamed Ibrahim Mosaad** [3,*] **and Abdelaziz Mahmoud Bouchelaghem** [1]

1   Industrial Mechanics Laboratory, Badji Mokhtar Annaba University, Box 12, Annaba 23000, Algeria
2   LGEB Laboratory, Department of Electrical Engineering, Biskra University, Biskra 07000, Algeria
3   Yanbu Industrial College (YIC), Alnahdah, Yanbu Al Sinaiyah, Yanbu 46452, Saudi Arabia
*   Correspondence: m_i_mosaad@hotmail.com or habibm@rcyci.edu.sa

Abstract: Knowledge of the distinctive frequencies and amplitudes of broken rotor bar (BRB) faults in the induction motor (IM) is essential for most fault diagnosis methods. Fast Fourier transform (FFT) is widely applied to diagnose the faults within BRBs. However, this method does not provide satisfactory results if it is applied directly to the stator current signal at low slip because a high-resolution spectrum is required to separate the different components of the frequency. To address this problem, this paper proposes an efficient method based on a Hilbert fast Fourier transform (HFFT) approach, which is used to extract the envelope from the stator current using the Hilbert transform (HT) at low slip. Then, the stator current envelope is analyzed using the fast Fourier transform (FFT) to obtain the amplitude and frequency of the particular harmonic. These data were recently collected and selected as BRB fault features and were employed as adaptive neuro-fuzzy inference system (ANFIS) inputs for BRB fault autodiagnosis and classification. To identify the BRB defect by determining the number of broken bars in the rotor, two ANFIS models are proposed: ANFIS grid partitioning (ANFIS-GP) and ANFIS-subtractive clustering (ANFIS-SC). To validate the effectiveness of the proposed method, three different motors were used during experiments under various loads; the first was with one broken bar, the second was with two adjacent broken bars, and the third was a healthy motor. The obtained results confirmed the effectiveness and the robustness of the proposed method, which is based on the combination of HFFT-ANFIS-SC to diagnose the BRB faults and quantify the number of broken bars under different load conditions (under low and high slip) precisely with minimal errors (this method had an MSE of 10-14 and 10-7 for the RMSE) compared to the method based on the combination of HFFT-ANFIS-GP.

Keywords: induction motor; broken rotor bars; Hilbert transform; adaptive neuro-fuzzy inference system; grid partitioning; subtractive clustering

1. Introduction

Induction motors (IMs) are well-known for their reliability as industrial drives. However, during operation, IMs are frequently subjected to hostile conditions, resulting in early deterioration or complete failure [1]. The faults of induction machines cause excessive downtime which generates large losses in terms of maintenance and lost revenues. Even a small fault can cause important losses, such as reducing efficiency and increasing temperature, which reduce the insulation lifetime, increase vibration, and reduce the bearing lifetime [2,3]. All earlier cited consequences are commonly due to the operating environment conditions and internal factors of the machines that can be summarized into three main categories, which are mechanical, electromagnetic, and thermal, causing the bar damages. In addition, Ayhala et al. [4] reported that the main failure cause is bending stress due to the electromagnetic forces generated by the action of slot linkage

flux. The squirrel cage induction motors suffer from a variety of mechanical and electrical faults, of which about 10% are broken rotor bar (BRB) faults [5]. BRB faults are one of the most common motor problems [1]. A BRB fault can be caused by either an imperfection in the manufacturing process or turbulent operating conditions, such as direct-on-line starting duty cycles, high thermal stresses, excessive pressures, high currents that occur in the motor cage, and pulsating mechanical loads [6]. Any asymmetry in the rotor of a squirrel cage induction motor presents unevenly distributed rotor currents. When a BRB occurs in one rotor bar, the current flowing through it is shifted to the other rotor bars, putting the adjacent bars under higher stress and potentially leading to more BBFs until the motor fails completely. The reactions of these currents to the air-gap field generate fault-specific signatures in the spectrum of the current, power, torque, and speed. For this reason, many researchers resorted to using signal processing approaches to extract the information through signal analysis techniques for the diagnosis operation, such as current, stator voltage, power, speed, temperature, and vibration signals [7–9]. For instance, motor current signature analysis (MCSA) is a widely used technique thanks to its low cost and noninvasive nature [10]. In the MCSA technique, the current signal of a running motor is collected and recorded. Then, the fault features are extracted from recorded data in the time domain, frequency domain, or time–frequency domain using signal processing techniques. Among the most commonly used signal processing tools for IM fault diagnosis in the literature are: fast Fourier transform (FFT), short-time Fourier transform (STFT), wavelet transform (WT) [9,11], and empirical mode decomposition (EMD) [12]. Generally speaking, FFT is an appropriate technique for BRB fault detection in the steady state [11,13]. However, the application of this technique has some limitations, which especially affect the diagnosis of BRB faults at low load or no load (low slip). From these limitations, the characteristics of the sideband components, $(1 \pm 2ks)f_s$ (s is the rotor slip, f_s is the fundamental frequency, and $k = 1, 2, 3 \dots$), are very close to the fundamental frequency component [9], and the normal spectral leakage can obscure frequency components characteristic of the fault [14]. High-resolution techniques such as the estimation of signal parameters via rotational invariance techniques (ESPRIT) and multiple signal classification (MUSIC), as presented in [15–17], have recently sparked a lot of attention. However, the precision of the utilized sensor has a major impact on those techniques, and a significant computing burden is necessary. Therefore, some development and adaptation of low-resolution BRB diagnosis techniques are preferred to using such high-resolution techniques.

The envelope of Hilbert transform (HT) with FFT (HFFT) is proposed in this paper to adopt the FFT technique. HT is used to obtain the envelope from the stator current in the transient regime and at the steady state of IM. Then, it is processed by the FFT. The envelope signal occupies the low-frequency spectral region, and its analysis offers better detection than that of the spectrum of the original signal, as the power frequency is eliminated from the signal [18]. This method gives good detection of the BRB fault, especially at low slip. Within the same framework, many researchers have focused on artificial intelligence (AI) techniques as powerful tools for motor fault classification and autodetection [9,19–25]. These tools do not require accurate modeling of the system, and they provide high efficiency in autodiagnosis. The vector features are extracted from fault detection techniques, and they are then used as inputs for AI tools such as fuzzy logic, neural networks, or combinations (neuro-fuzzy networks) for fault recognition [26]. The combination of diagnostic techniques and AI tools has permitted great developments in the field of the monitoring and maintenance of industrial machines and processes with optimal effort and an effective cost.

Some recent works involve BRB detection without a classifier in Refs. [27,28]. One can see successive variable mode decomposition (SVMD) for BRB detection in IMs. Based on signal energy, the stator starting current is used. Then, a quadratic regression curve method is utilized in order to achieve the detection objective. A cyclic modulation spectral analysis of vibratory signals was proposed by Zuolu Wang et al. [28], and the obtained results show the efficiency of the proposed method for BRB fault identification. However, regarding the

nature of the signal used, the earlier detection of faults is questionable since mechanical signals are less sensitive compared to electrical signals. However, a considerable amount of literature has examined the diagnosis and classification of BRB faults in IMs. In [29], the authors presented an experimental diagnosis study about BRB faults in IMs based on the HFFT method of the stator current using a fuzzy system. They used two features extracted from the HFFT method, namely, the amplitude of the $2sf_s$ harmonic and the DC value. These features were used as the inputs of the fuzzy logic system for the decision making about the rotor state. Gyftakis et al. [30] proposed an innovative diagnostic method based on Park's vector approach to detect BRB faults in IMs. The method consists of the monitoring of the higher harmonic index after applying elliptical and notch filters on the Park's vector components of the stator currents. The filtered Park's vector modulus is calculated and processed by the FFT to detect the fault by giving the amplitudes of the $2ksfs$ signatures. It is noted that this method and the HFFT approach give the same spectrum of the BRB fault, which is equal to $2skfs$. However, the filtered Park's vector method needs three current sensors to be carried out, whereas the HFFT method needs only one sensor. Furthermore, in Ref. [11] one can see a hybrid diagnosis approach based on Hilbert and discrete wavelet transform (HDWT) for BRB faults in IMs. The proposed method used the HT to obtain a stator current envelope to be processed via DWT. This work has a significant result, but the WT has some drawbacks, including the arbitrary selection of the mother wavelet, which may introduce an inappropriate fault detection [18]. Harzelli et al., in [9], presented a method for the diagnosis of simple and mixed BRBs and stator short-circuit faults in the closed-loop drive for IMs. The authors adopted two strategies: The first was based on the model used to generate a residual speed signal to indicate the presence of possible failures using the high-gain observer in the closed-loop drive. The second was based on HFFT. The amplitude and frequency of the harmonic $2sf_s$ extracted from the HFFT were used as fault indicators and were considered as inputs for the neural network (NN) in order to identify serval possible faults and distinguish between them. In the work conducted by [19], the authors applied the support vector machine (SVM) and an NN to diagnose BRBs and to show faults in IMs based on the vibration and the instantaneous power signals of IMs. In both cases, the dimensionality of the signals was reduced using principal component analysis (PCA), and the selected features were then sorted in order of importance using the sequential floating forward selection (SFFS) approach to reduce the number of input features and discover the most ideal feature set. The chosen features were then classified by the SVM and ANN methods. The obtained results revealed that ANN performs better than SVM. Despite the good technical aspects of the proposed approach, it remains costly because of its calculation complexity. Furthermore, in Ref [22] the researchers proposed a simulation-based study in which a combination of the HFFT and an NN was proposed to detect and quantify the number of broken bars in the rotors of IMs under various load conditions. The amplitudes and frequencies of the $2sf_s$ harmonic were extracted from HFFT as fault indicators to build the NN for autodiagnosis purposes. Despite the effectiveness of this approach, it is still insufficient to confirm its applicability. For that, an experimental test should be carried out. One can also find other BRB detection approaches, such as the inverse thresholding to spectrogram method presented in Ref. [31]. A simulation performed under ANSYS Maxwell 2D led to efficient BRB detection. An interpolated kernel density estimate for IM diagnosis was proposed in Ref. [32], where the fault signature was extracted from the vibration signal. In Ref. [33], a DWT + fuzzy incipient BRB detection was proposed. The method provides higher efficiency, but the optimization of fuzzy MFs and the selection of appropriate IF–THEN rules governing the fuzzy inference system is a complex task. In Ref. [34], a CWT + PCA+ ANFIS diagnostic algorithm was proposed. The simulation results showed that the algorithm performs well in the presence of PCA. However, based on the nature of signal processing techniques, it is well-known that continuous wavelet transform requires substantial time and CPU capacity compared to the discrete technique. In addition, the use of five parallel ANFISs increases the computational complexity of the detection algorithm compared to the other

techniques. In Ref. [35], the authors proposed an ANFIS classifier based on stator current Id and Iq under different loads. Although the obtained results seem efficient, their validation in practice is still debatable since temporal stator current signals do not provide explicit information about motor reliability. In Ref. [36], Merabet et al. proposed a multimesh model based on a BRB detection approach of three phases of IMs. the signal processing technique used was the wavelet packet method. The use of the ANFIS classifier proves its effectiveness. However, experimental validation is still necessary in order to evaluate the consistency of the proposed WP + ANFIS technique. Dias et al. [37] proposed an experimental FFT + ANFIS BRB diagnosis of IMs. The main important experimental contribution was the use of three faulty scenarios, which were one BB, two adjacent BRBs, and two nonadjacent BRBs. Regarding the ANFIS classifier, a grid partitioning identification method was used in order to build the initial fuzzy inference system (FIS). The obtained results show the efficiency of the proposed method, even at very low slip. However, the main drawbacks of that method are the number of modifiable parameters when the number of inputs is ≥6 and that selected MFs are important, which requires high computational performance in order to perform the training phase. In Ref. [38], the authors proposed an FFT + fuzzy BRB detection of squirrel cage induction motors. The advantage of this method is that the developed multiwinding model of IMs includes four BRBs and correctly detects the nature of faults based on the FFT of the current signals, which allows the extraction of amplitude $(1 \pm 2s)$ *fs* harmonics. However, a lack of experimental validation and the nature of the classifier, which requires trial-and-error tuning based on human expertise, are the most relevant drawbacks. In a major advance in BRB detection algorithms, Mikko Tahkola et al. [39] developed an ATSC- NEX algorithm. The results show the effectiveness of this automated machine learning algorithm in correctly evaluating the state of IM rotor bars. The main advantage of ATSC- NEX is the autoconstruction of the model and its ability to overcome the overfitting phenomenon thanks to the introduced early stopping criterion. However, the optimization of the hyperparameters is the main disadvantage of the algorithm. Even if nested cross-validation provides good results at present, the optimization is still computationally expensive.

Generally, the summary of a fault diagnosis planner is data (or signal) acquisition, feature extraction, and classification [40]. Relevant to the aforementioned studies, the present work introduces a new approach in which the HFFT method is applied to the stator current with the ANFIS to detect and identify the number of broken bars in the rotor under different conditions. The proposed approach offers the advantage of providing a data-driven diagnostic model that can attain the objectives in question without the necessity of a complex mathematical model. The ANFIS is a specific type of neuro-fuzzy classifier approach integrating the NN adaptive capability and the fuzzy logic qualitative approach. It has been successfully applied for automated fault detection and diagnosis in IMs [41].

The main contributions of this study are as follows:

- A new combined HFFT-ANFIS is proposed as an effective real-time diagnosis method to detect BRB faults in IMs.
- Two ANFIS models, namely, grid partitioning (GP) and subtractive clustering (SC), are suggested and validated through experiments for the detection of BRB faults.

The proposed HFFT-ANFIS-GP and HFFT-ANFIS-SC models were carried out and validated based on experimental results aiming at detecting and quantifying the broken bar numbers under different conditions. The HFFT approach was applied through HT, which is used to extract the stator current envelope and process it by FFT. The frequency and the amplitude of the $2sf_s$ harmonic extracted from the HFFT were used as BRB fault indicators and considered as the ANFIS input for autodetection.

This paper is structured as follows: In Section 2, a description of the HFFT technique and the adaptive neuro-fuzzy system are presented. In Section 3, the methodology of fault detection is proposed. A description of the test bench and the experimental test is presented in Section 4. In Section 5, the experimental results and discussions are introduced, and the conclusion is presented in Section 6.

2. Theoretical Description

2.1. Hilbert Fast Fourier Transform Technique (HFFT)

HFFT is a signal analysis technique that is based on extracting the envelope from the stator current signal by HT and then processing it via FFT. This technique has proven its effectiveness when applied to the diagnosis of the rotating machines in both states, stationary and nonstationary signals. The HT is defined as a convolution of the signal $x(t)$ with the function $1/t$. Therefore:

$$
\begin{aligned}
HT(x(t)) &= y(t) \\
&= \frac{1}{\pi.t} \times x(t) \\
&= \frac{1}{\pi} \int_{-\infty}^{+\infty} \frac{x(\tau)}{t-\tau} d\tau
\end{aligned}
\tag{1}
$$

where $y(t)$ represents the HT of the temporal signal, $x(t)$. In addition, based on the Cauchy principal value, the convergence $t = \tau$ is permitted [22].

The HT of a signal, $x(t)$, can be written in the following form [42]:

$$
\begin{aligned}
\vec{x}(t) &= x(t) + jy(t) \\
&= A(t)e^{j\varphi(t)}
\end{aligned}
\tag{2}
$$

The signal $\vec{x}(t)$ is called the analytic signal. The amplitude modulation, $A(t)$, of the time signal is the instantaneous amplitude of $\vec{x}(t)$, and it is calculated using the following relation:

$$
A(t) = \sqrt{x(t)^2 + y(t)^2}
\tag{3}
$$

The phase modulation, $\varphi(t)$, can be determined as:

$$
\varphi(t) = \arctan\left(\frac{y(t)}{x(t)}\right)
\tag{4}
$$

The computation of the analytic signal modulus, $\vec{x}(t)$, gives the envelope of the signal.

The FFT is used in diagnosis to extract the components of the different spectra concerning the IM faults from the signals. Unfortunately, this approach was not able to provide good information at low slip because the frequency components may be obscured by an overlap with the fundamental frequency, especially in a BRB fault, as shown in Figure 1a. The HFFT is used as a solution to this problem (Figure 1b). Furthermore, it has good features for the diagnosis of faults in IMs, as [42]:

- The positive frequency value of the original signal is maintained, while negative frequencies are canceled.
- The amplitude, $A(t)$, contains the low frequencies of the original signal and the high frequencies in the phase, $\varphi(t)$, of the analytical signal.
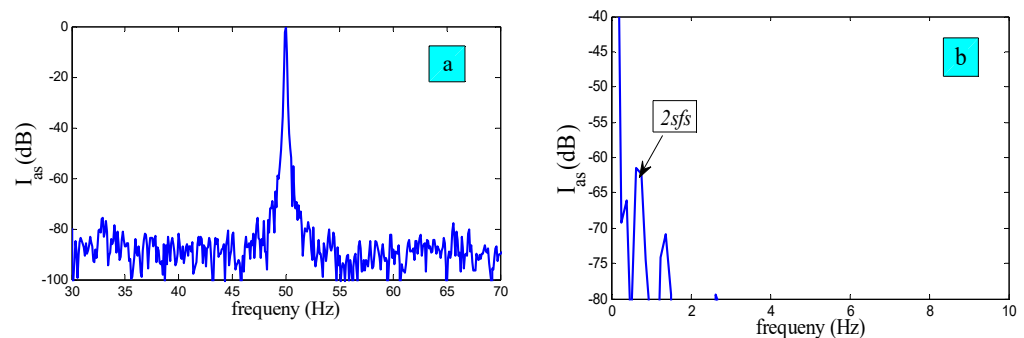

Figure 1. Analysis of the stator current signal for IM with two broken bar faults under low load by: (**a**) FFT; (**b**) HFFT.

In the present study, the HFFT was applied on the stator current in order to detect the side bands of the frequency components of the BRB fault, even at low slip, where the characteristic frequency of this fault is $2skf_s$ and $k = 1, 2, 3 \ldots, n$.

2.2. Adaptive Neuro-Fuzzy Inference System (ANFIS)

The ANFIS is a combination of fuzzy logic and a neural network algorithm, initially proposed in the early 90s by J S Jang [43]. It combines the greatest features of both because it offers fuzzy logic qualitative analysis as well as learning skills. The hybrid learning rule is applied by ANFIS to optimize the final inference system through the NN's training. ANFIS is equivalent to a first-order Takagi Sugeno system [43]. It is represented by the following two IF–THEN rules:

$$1^{st} \ rule : IF \ x \ is \ A_1 \ and \ y \ is \ B_1 \ THEN \ f_1 = p_1 x + q_1 y + r_1 \tag{5}$$

$$2^{nd} \ rule : IF \ x \ is \ A_1 \ and \ y \ is \ B_1 \ THEN \ f_2 = p_2 x + q_2 y + r_2 \tag{6}$$

where x and y denote system inputs. A_i and B_i are fuzzy subsets coded by fuzzy membership functions (MFs), and f_i are system outputs within the fuzzy layer and are based on fuzzy IF–THEN rules. p_1 and f_1 are linear adaptive parameters that are tuned during the training phase.

The ANFIS flowchart is shown in Figure 2. It consists of five layers, where three layers are fixed nodes schematized by circles and two adaptive layers are schematized by squares.
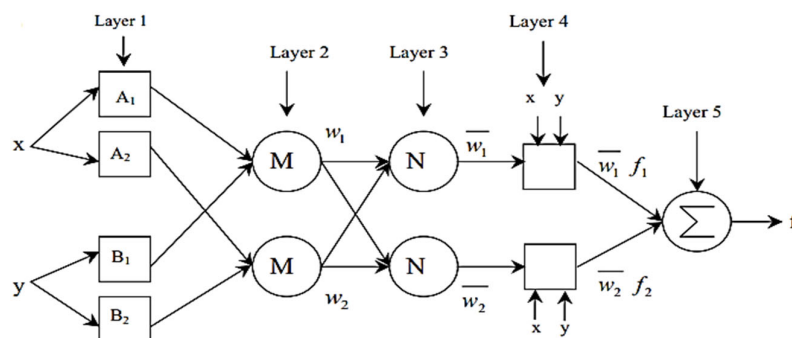

Figure 2. Flowchart of the ANFIS system.

Fuzzification layer: A subset of adaptive nodes expressing the fuzzy membership conditions of each input, where:

$$O_i^1 = U_{A_i}(x) \tag{7}$$

where x denotes the input to the node i, A_i denotes the linguistic label associated with the node i, and U_{A_i} is a membership function (MF). In this study, the Gaussian membership function given by (8) is used:

$$U_{A_i}(x) = e^{-\frac{1}{2}\left(\frac{x-c}{\sigma}\right)^2} \tag{8}$$

The Gaussian MF is fully defined by two nonlinear parameters, c and σ, where c is the MF center and c determines the Gaussian MF width. These nonlinear parameters are known as premise parameters and are adjusted during the training phase [43,44].

Product layer: a subset of fixed nodes that produces the firing strengths of the rules and acts as a simple multiplier of signals received from the previous layer as:

$$W_i = U_{A_i}(x) \times U_{B_i}(x) \tag{9}$$

Normalization layer: a subset of fixed nodes that normalizes each weight, W_i, by dividing it according to the total of all the weights associated with each rule as follows:

$$\overline{W} = \frac{W_i}{W_1 + W_2}, i = 1, 2 \tag{10}$$

W is called normalized firing strengths [43,44].

Defuzzification layer: the output of each node given by (9) is the product of each normalized firing strength and a first-order polynomial:

$$O_i^4 = \overline{W} f_i = \overline{W_i(p_i x + q_i y + r_i)} \tag{11}$$

where $\{p_i, q_i, r_i\}$ are the consequent parameters to be defined during the training phase [43,44].

Output layer: a single layer of fixed nodes that sums all received information from the previous layer and delivers the network output, such as [43,44]:

$$O_i^5 = \sum \overline{W} f_i \tag{12}$$

In the present research, a hybrid training algorithm is used to adapt the network parameters. The hybrid algorithm is a two-pass algorithm combining the least-squares method and the backpropagation gradient descent method to optimize the premise and the consequent parameters [45,46].

The first step of ANFIS model construction is the construction of an initial FIS system, which can be built using different identification methods. In this paper, grid partitioning (GP) and subtractive clustering (SC) are used to achieve the objectives.

(a)　ANFIS with Grid partitioning

The grid partitioning identification method consists of dividing the data space into an equally spaced grid. For this purpose, the number of grid nodes in the dataset space is defined by the experience of the user by assigning a determined number of MFs to each entry. The grid partitioning method is recommended for systems with a small amount of data. One of its major disadvantages is that the network may become too large, depending on the number of MFs. Hence, the need for high-performance machines to envisage the training phase is necessary [45].

(b)　ANFIS with Subtractive clustering

Subtractive clustering is an optimization approach used to build the initial FIS network for the ANFIS network. This three-step algorithm has the advantage of making the calculation straight forward, so time is potentially reduced. It enables the center and radius of each cluster to be determined based on the data. They are then used to generate the MFs responsible for the transition to the fuzzy domain (fuzzification).

1st Step: For particle collection dataset A with n data points in M-dimensional space, $A = \{X_i, \dots, X_n\}_{i=1}^n$, in which each dataset's element represents a candidate for the cluster center. The density measurement is given as follows:

$$D_i = \sum_{i=1}^n \exp\left\{ -\frac{\|x_i - x_j\|^2}{\left(\frac{r_a}{2}\right)^2} \right\} \tag{13}$$

where r_a is a positive constant. For the density measurement, a density value at a given point is systematically high if the amount of data within the radius r_a is high and vice versa.

2nd step: Based on the density measurement described in the first step. The center of the first cluster is assigned to the point with the highest density. Taking r_b as the new cluster radius, the density measurement of each point is revised as follows:

$$\overbrace{D_i}^{Revised} = D_i - D_{c_i} \exp\left\{ -\frac{\|x_i - x_j\|^2}{\left(\frac{r_a}{2}\right)^2} \right\} \tag{14}$$

where D_{c_i} is the revised density measurement.

3rd step: Finally, the cluster center Xc_2 is fixed according to the density calculations of all data points. All calculations are continuously performed until a sufficient number of cluster centers are generated [47,48].

(c)   Performance Criteria

In this work, both training and testing errors can be evaluated by the mean- square error (*MSE*) and the root-mean-square error (*RMSE*) for the ANFIS model validation and to determine the performance of the models predicted by the output values of the corresponding dataset:

$$MSE = \frac{1}{n}\sum_{i=0}^{n}(X_i - Y_i)^2 \tag{15}$$

$$RMSE = \sqrt{\frac{1}{n}\sum_{i=0}^{n}(X_i - Y_i)^2} \tag{16}$$

where n is the number of samples and X_i and Y_i are the measured and predicted values, respectively.

3. Experimental Methodology

The general framework of the proposed diagnosis methodology is shown in Figure 3. First, the stator current signal under different test conditions was acquired. Next, The HFFT was applied to the acquired signal, which extracted the envelope of the current signal by HT then processed it via FFT. The amplitude A_{bb} and the frequency f_{bb} corresponding to the $2sf_s$ harmonic were selected as BRB fault features. To classify the fault, the numbers of broken bars were determined through the use of two models of ANFIS (GP and SC) where the A_{bb} and f_{bb} were considered as inputs of the ANFIS models. The results of the ANFIS models were compared to determine which model's performance was better along with the convergence between them.
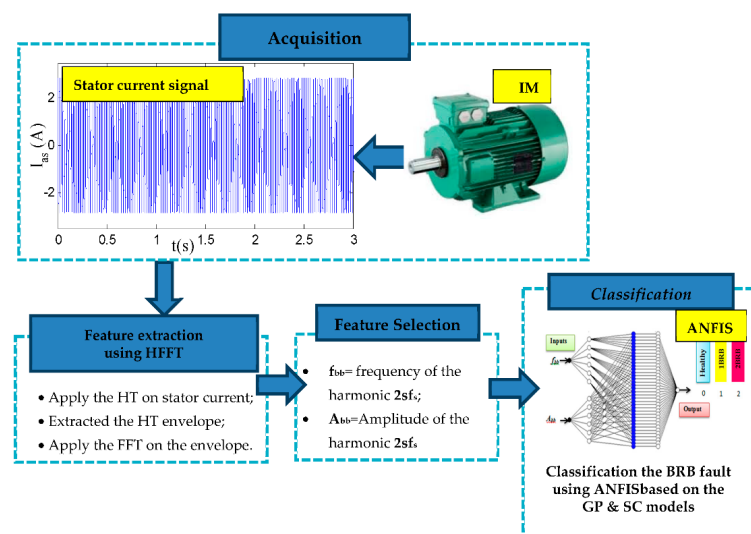

Figure 3. General framework for fault detection methodology.

4. Experimental Test

4.1. Description of the Test Bench

The experimental setup of this research is depicted in Figures 4 and 5. Figure 4 represents the descriptive flowchart of the experimental setup, and Figure 5 shows the real experimental setup. A series of tests were conducted on three squirrel-cage induction motors that each had a nominal power of 1.1 kW, 230/400 V nominal voltage, and a rated speed (N) of 1450 rpm. One motor was considered as a reference healthy motor. The other two motors were tested with one broken bar and two adjacent broken bar faults. The parameters of the tested motors are given in Table 1.
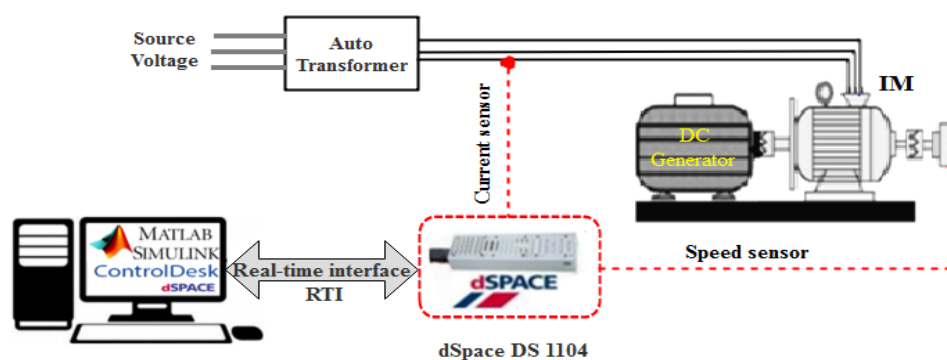
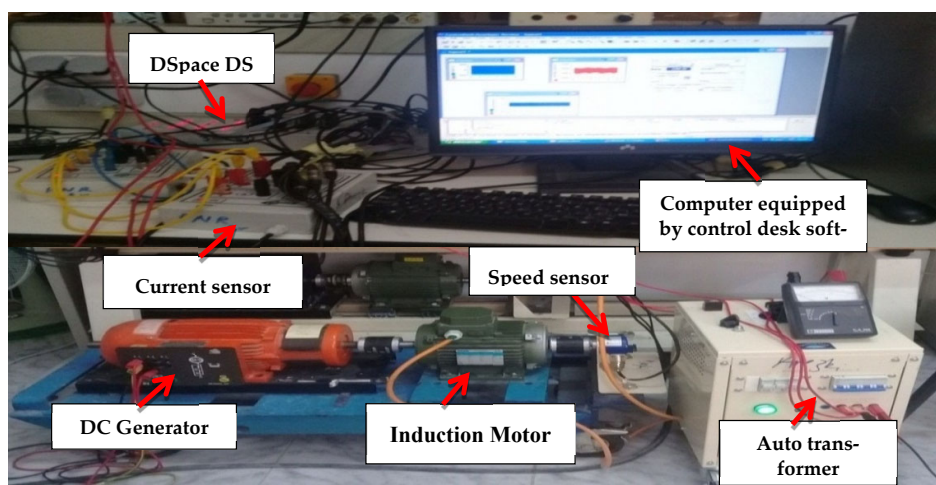**Figure 4.** Descriptive flowchart of the experimental setup.

Figure 5. Experimental test bench.

Table 1. Specification of the IMs used.

Characteristics	Specification
Rated Power	1.1 (kW)
Rated Voltage	400/230 (V)
Rated Current	2.5 (A)
Supply Frequency	50 (Hz)
Number of Poles	4
Rated Speed	1450 (rpm)
Number of Rotor Bars	46

The power supply used was a three-phase autotransformer (0–450 Vrms line-to-line) that directly fed the IM (400 V, 50 Hz, Y). The mechanical load was applied to the IM by connecting the shaft to a DC generator of 1 kW rated power. The output of the DC generator was connected to a variable resistive load to allow tests to be performed at different loads. The measurements in the IM were carried out using the incremental speed sensor and a current sensor connected to the stator. Data acquisition was performed using the DSpace 1104 card with a TMS32F240 DSP via Control Desk software. The sampling frequency of the data acquisition was 10 kHz in all conducted experiments. For the laboratory tests, the BRB faults were performed by drilling a small hole of $\varnothing = 3$ (mm) and a depth of $e = 2$ (mm) at the rotor bar, as shown in Figure 6.
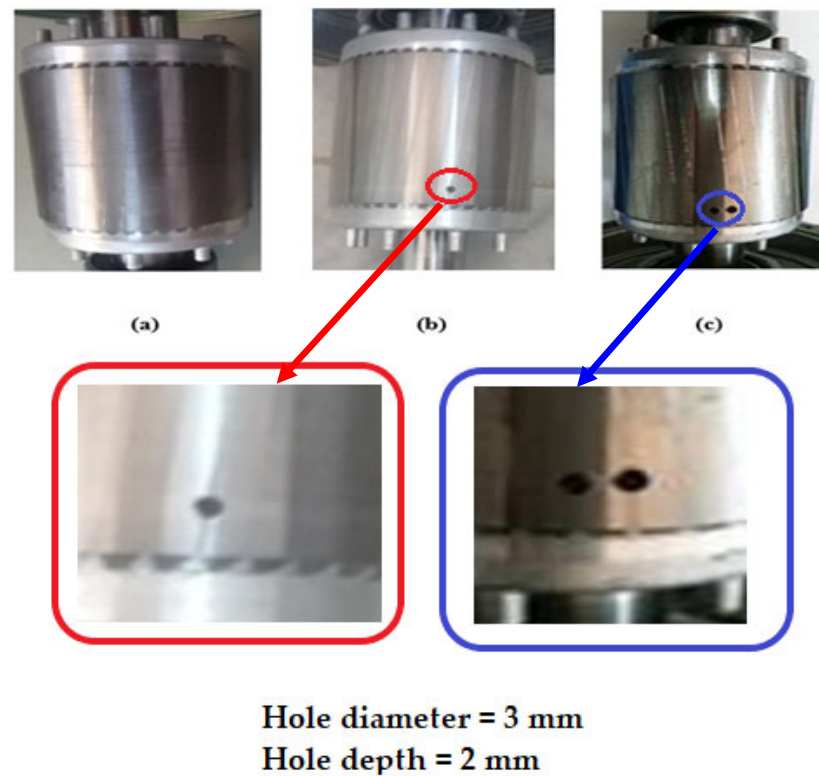
Hole diameter = 3 mm
Hole depth = 2 mm

Figure 6. The rotors used in experimental tests: (**a**) healthy; (**b**) one broken bar (1BRB); (**c**) two adjacent broken bars (2BRB).

Figure 7 represents a detailed flowchart of the proposed approach. As a data-driven method, data collection and processing are essential for detecting and determining the number of broken bars in the rotor of an IM. The proposed approach was implemented, and it is shown below as follows:

(a) *Acquisition*: the stator current (I_s) under different conditions was acquired using the current sensor, which was connected to the interface of the DSpace card to record the data on the PC.

(b) *Applying the HFFT method*: using Matlab software, the HFFT was applied to the acquired signal by extracting the envelope of the current (Is envelope) by HT then processing it via FFT.

(c) The amplitude (A_{bb}) and the frequency (f_{bb}) corresponding to the $2sf_s$ harmonic (extracted from Is_envlope) were chosen as BRB fault indicators.

(d) *Classification of the BRB fault*: using the two ANFIS models, GP and SC, the classification of the fault was performed by quantifying the number of broken bars in the rotor of an IM, where the amplitude (A_{bb}) and the frequency (f_{bb}) were considered as the inputs of the two ANFIS models and the number of the broken bars was the desired output.

The total number of samples forming (input/output) couples was 132. All samples were carefully divided, where 105 were used for training and 27 were used for testing.

(e) *Accuracy evaluation*: in order to evaluate the efficiency and performances of the ANFIS models, the MSE and RMSE were chosen to be the indicators of accuracy, as explained in Section 2.2.
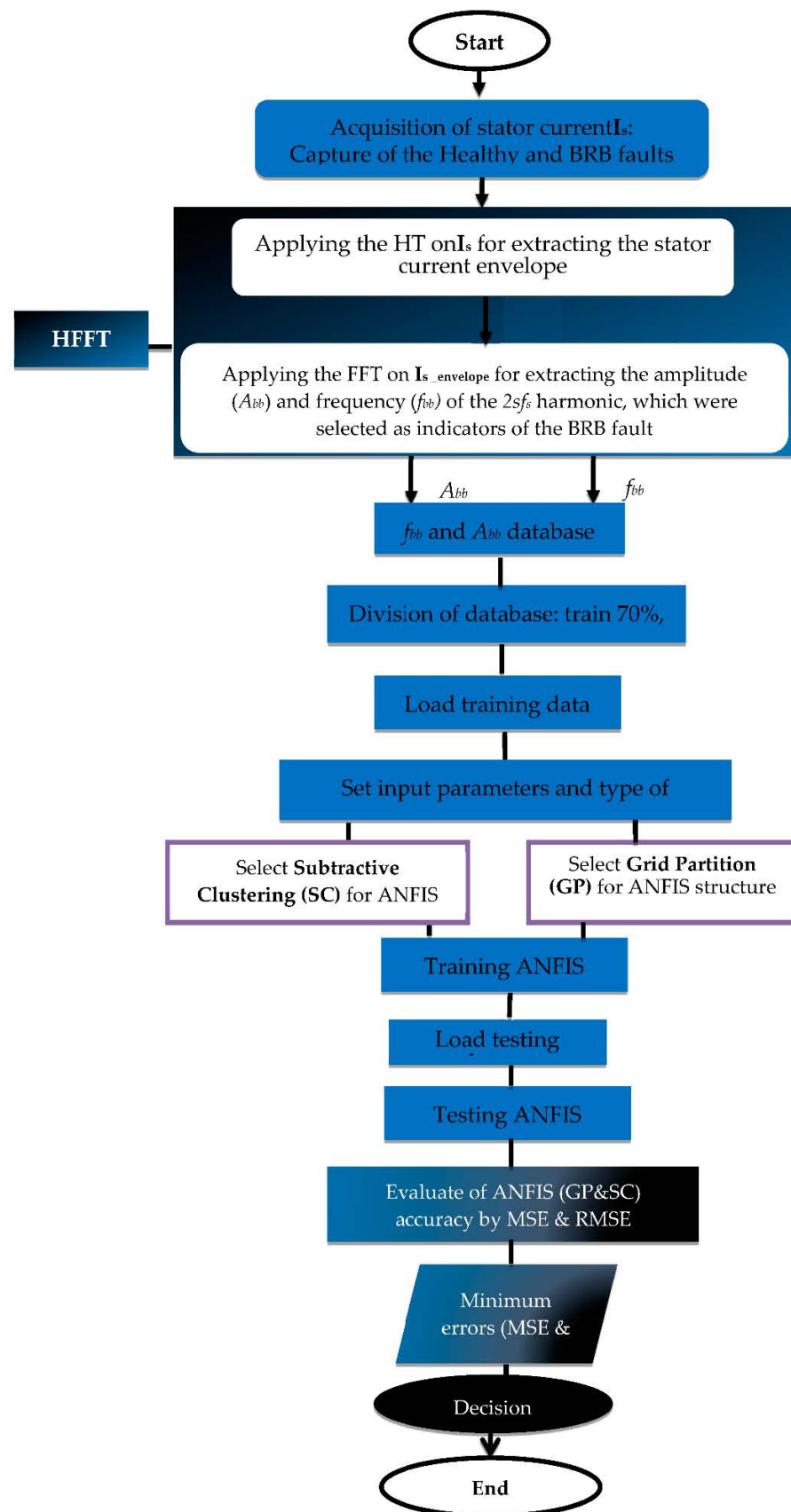
Start

Acquisition of stator current**I$_s$**:
Capture of the Healthy and BRB faults

Applying the HT on**I$_s$** for extracting the stator current envelope

HFFT

Applying the FFT on **I$_{s\_envelope}$** for extracting the amplitude (A_{bb}) and frequency (f_{bb}) of the *2sf$_s$* harmonic, which were selected as indicators of the BRB fault

A_{bb} f_{bb}

f_{bb} and A_{bb} database

Division of database: train 70%,

Load training data

Set input parameters and type of

Select **Subtractive Clustering (SC)** for ANFIS

Select **Grid Partition (GP)** for ANFIS structure

Training ANFIS

Load testing

Testing ANFIS

Evaluate of ANFIS (GP&SC) accuracy by MSE & RMSE

Minimum errors (MSE &

Decision

End

Figure 7. Flowchart of the experimental method of the "HFFT-ANFIS" approach.

4.2. Selection of the ANFIS Model Parameters

The two proposed ANFIS models, namely, ANFIS-GP and ANFIS-SC, were developed using data collected from the experimental measurements being summarized in Table 2; the dataset was divided carefully into training and testing subsets, as presented in Section 5. The training dataset was used to train the ANFIS-GP and ANFIS-SC models, whereas the testing dataset was used to verify the accuracy and the effectiveness of the trained ANFIS models. Although the training data size was small, it was of good quality and it described with high fidelity the dynamics of the system. Moreover, the considered experimental scenarios can help us make the optimal decision about the condition of the bars in the rotor of an IM and therefore detect and classify BRB faults.

Table 2. Quantitative analysis of the generated dataset.

	Load	Healthy	1BRB	2BRB	Number of Conducted Experiments	Training	Testing
	10	●	●	●	5×3	●	
	20	●	●	●	5×3	●	
	30	●	●	●	3×3		●
	40	●	●	●	5×3	●	
Input	50	●	●	●	5×3	●	
	60	●	●	●	3×3		●
	70	●	●	●	5×3	●	
	80	●	●	●	5×3	●	
	90	●	●	●	3×3		●
	100	●	●	●	5×3	●	
Output	-	0	1	2	-	-	-
Total	-	44	44	44	**132**	105	27

The first proposed ANFIS model is ANFIS-GP, which is based on dividing the data space into several square components, as mentioned earlier. The ANFIS-GP parameters are composed of two variable inputs, which are the frequency f_{bb} (I_1) and the amplitude A_{bb}(I_2) of the $2sf_s$ harmonic, and one variable output, the number of broken bars in the rotor. A linear fuzzy output with six Gaussian-type membership functions (MFs) was used, as shown in Figure 8, where the two inputs were fuzzified by six Gaussian fuzzy sets directed by 36 significant IF–THEN rules, as shown in Figure 9. The modified parameters of ANFIS-GP were optimized using the hybrid training algorithm. The number of training epochs used was 100 because it was inferred that increasing the number of epochs did not lead to a better error.

The second ANFIS model is ANFIS-SC whose parameters are composed of the same inputs and output as the first model, with 25 Gaussian-type membership functions (MFs), as shown in Figure 10. The number of fuzzy rules used was 25 (see Figure 11). To generate these rules using the subtractive clustering technique, it was essential to determine the appropriate values of the parameters "accept ratio", "reject ratio", "squash factor", and "cluster radius". The performance of the ANFIS-SC model is very sensitive to the "cluster radius" parameter, while the rest of the parameters do not have a great influence. In this work, 'squash factor', 'accept ratio', and 'reject ratio' were considered to be 1.25, 0.5, and 0.15, respectively, while the cluster radius was equal to 0.1.
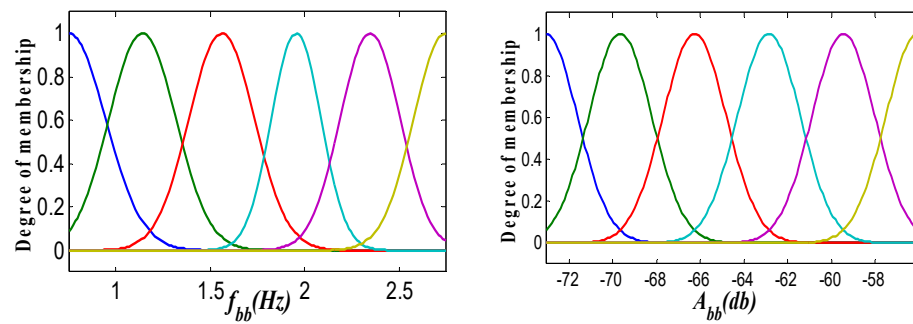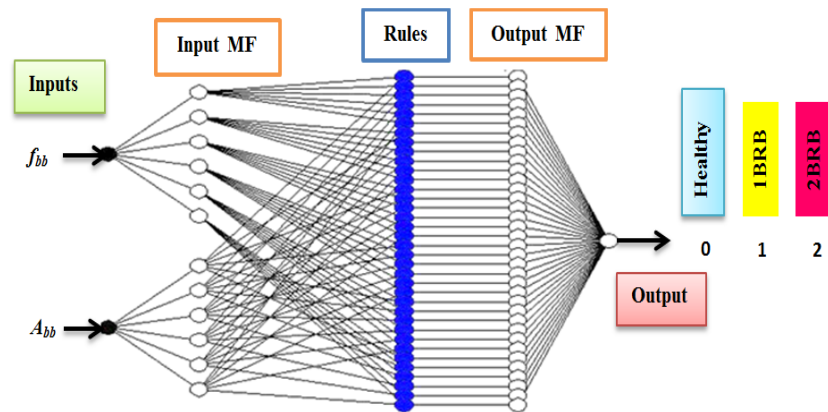
Figure 8. MFs obtained by ANFIS-GP model.

Figure 9. ANFIS-GP structure for BRB fault detection.
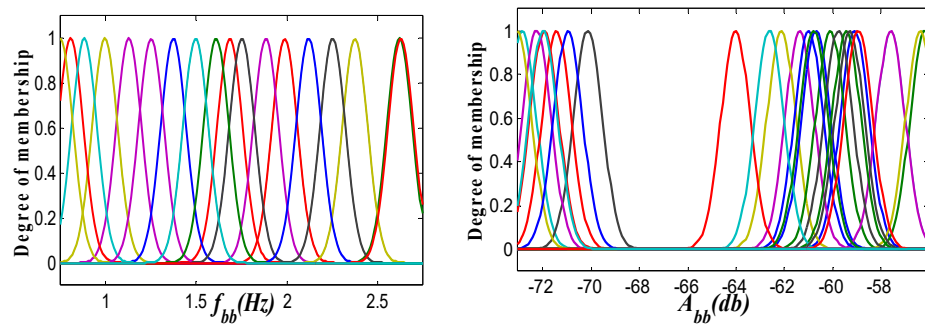

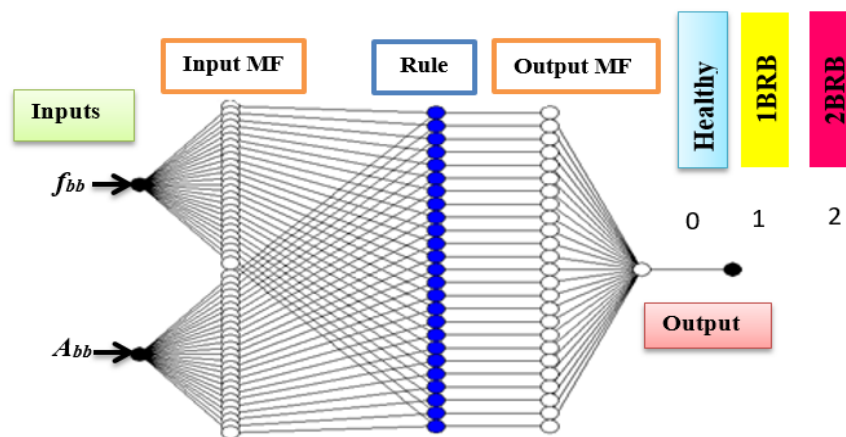**Figure 10.** MFs obtained by ANFIS-SC model.

Figure 11. ANFIS-SC structure for BRB fault detection.

The MSE and RMSE were finally calculated to select the best-suited parameters. The parameters of the two ANFIS models were used, and they are summarized in Table 3.

Table 3. Parameters of the two proposed ANFIS models.

ANFIS Parameters	ANFIS-GP	ANFIS-SC
Number of inputs	2	1
Number of outputs	2	1
Type of inputs' MFs	Gaussian	Gaussian
Fuzzy output type	Linear	Linear
Number of fuzzy rules	36	25
Number of learning iterations	100	100

In this study, the two ANFIS models were developed using MATLAB R2013b and Fuzzy Control Toolbox using a 2.10 GHz core i3 processor with 4 GB of RAM.

5. Experimental Results and Discussion

The experimental findings of the suggested diagnostic approach are provided in this section using the HFFT method on the stator current to extract fault indicators and then classify the fault using the two ANFIS models.

5.1. Application the HFFT Technique on the Stator Current

(a)   Stator current envelope

Figure 12 represents the experimental result of the stator current with its envelope for two BRB faults in an IM. The BRB fault caused the deformation of the magnetic field in the air gap of the IM, resulting in sequential modulation in the stator currents. This modulation of the stator currents is the so-called "envelope", which is repeated cyclically at a rate equal to double the slip frequency (2 sf$_s$). Typically, HT is used to extract the envelope from the current signal to detect this fault.
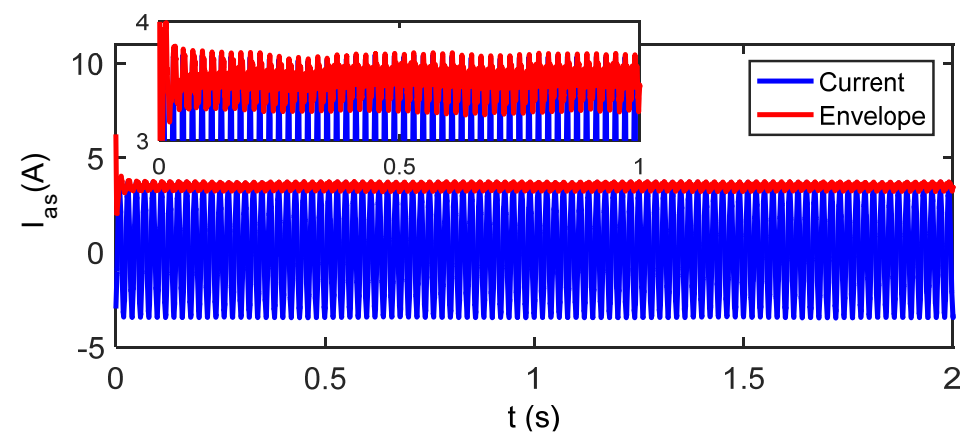

Figure 12. Stator current and its envelope for two broken rotor bars.

(b)   Envelope processing using FFT

Figure 13a,c represent the experimental results of the spectrum analyses of the stator current envelope in phase a$_s$ for healthy and faulty (1 BRB and 2 BRB) states under three different loads: low load, half load, and full load.
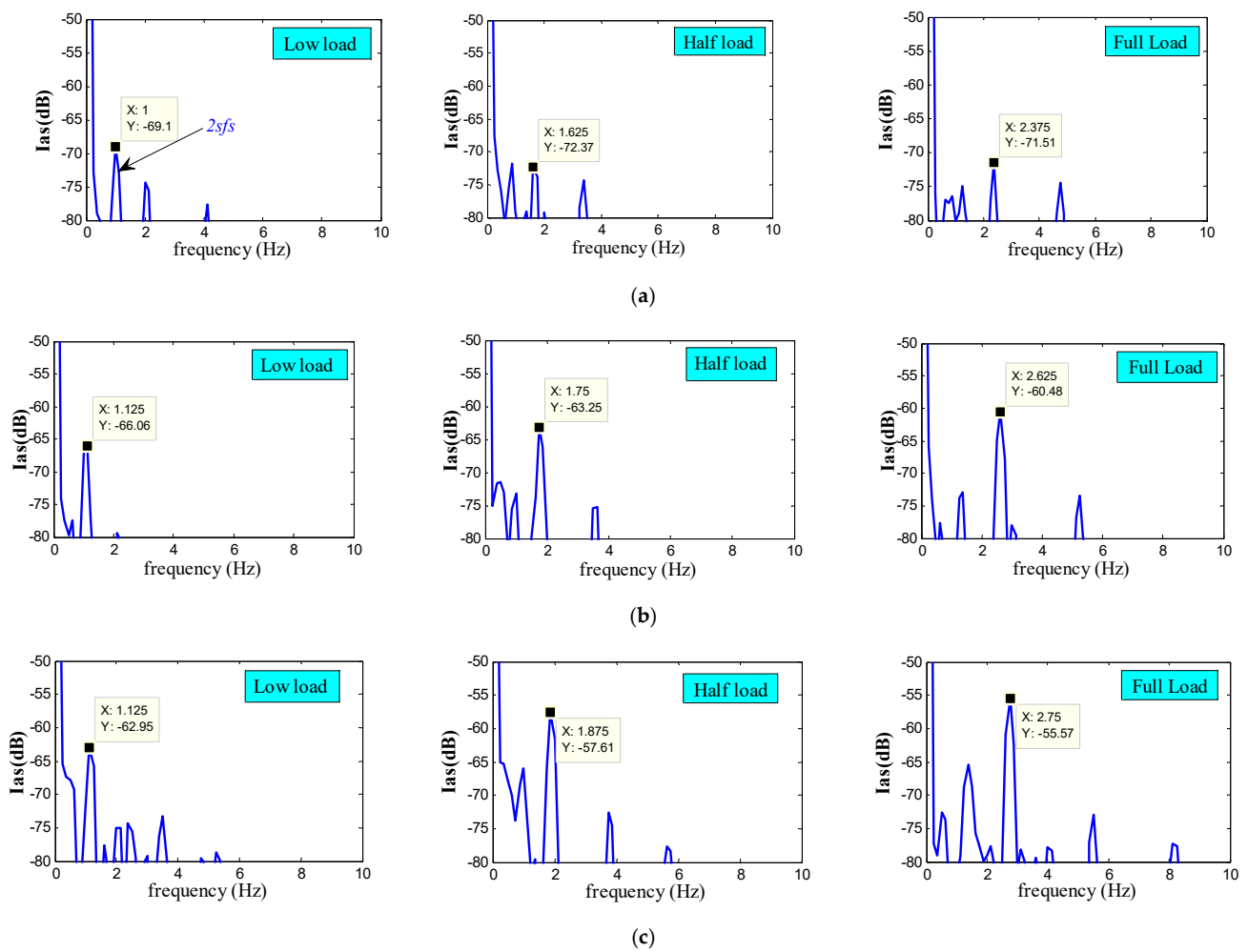
Figure 13. Spectra of stator current envelopes under different loads (low load, half load, and full load) for the states: (**a**) healthy; (**b**) one BRB fault; (**c**) two BRB faults.

In the healthy state, shown in Figure 13a, it was observed that the presence of the $2sf_s$ harmonic with a small amplitude corresponded to that created by the BRB defect. The appearance of this harmonic was the result of the natural asymmetry of the rotor. For example, bubbles in the rotor bars during the molding stage generated a slight disturbance in the distribution of magnetic flux in the air gap.

In faulty states (Figure 13b,c), it was observed that both the frequency and the amplitude of the $2sf_s$ harmonic are considerably affected by the BRB fault, and there was a direct relationship between the two features (the frequency and amplitude) and the number of broken bars. Moreover, they provided effective detection of the BRB fault in different conditions, even at low loads. These results have been proven by many studies, such as [9,18,22,29].

5.2. ANFIS-Based BRB Fault Diagnosis System

In all data-driven approaches, model construction is conducted based on training, which ensures the mapping between the **X** matrix-forming inputs and the **Y** matrix taken as an output. To attain a high-accuracy data-driven model, collected data should describe the dynamic of the modeled system or phenomenon [24,45,49]. Regarding that necessity and taking the objective of building an ANFIS classifier for BRB fault detection, three motors with three states were used, as explained in Section 4. Then, the fault signature collected for the HFFT of the current signal was considered as an input for ANFIS, while the output was constructed based on the known state of the motor. In order to construct a high-fidelity

classifier, the dynamic of the IM should be known. Therefore, serval experiments were carried out by varying IM loads from 10% to a rated load, with the same sampling frequency of 10 Hz. Table 2 summarizes a quantitative presentation of the built dataset. In the next subsections, the training and testing procedures are presented.

(a)   Training phase

The training dataset creation is of crucial importance for ANFIS development. To achieve the objectives, the training data should contain enough information, including several scenarios of the operation motor in the healthy and BRB fault states under different loads. To conduct the training phase of the proposed ANFIS models (GP and SC), as presented in Table 2, 105 samples were used by taking $\mathbf{I} = [f_{bb}, A_{bb}]$ as the input and the number of broken bars in the rotor as the output. The input dataset represented in Figure 14 is constituted by a series of samples (105) composed of five parts, with each part representing three states of IM operating conditions under seven loads as follows: 7×5 samples of a healthy motor under varying loads (10%, 20%, 40%, 50%, 70%, 80%, and 100%) of the rated load;
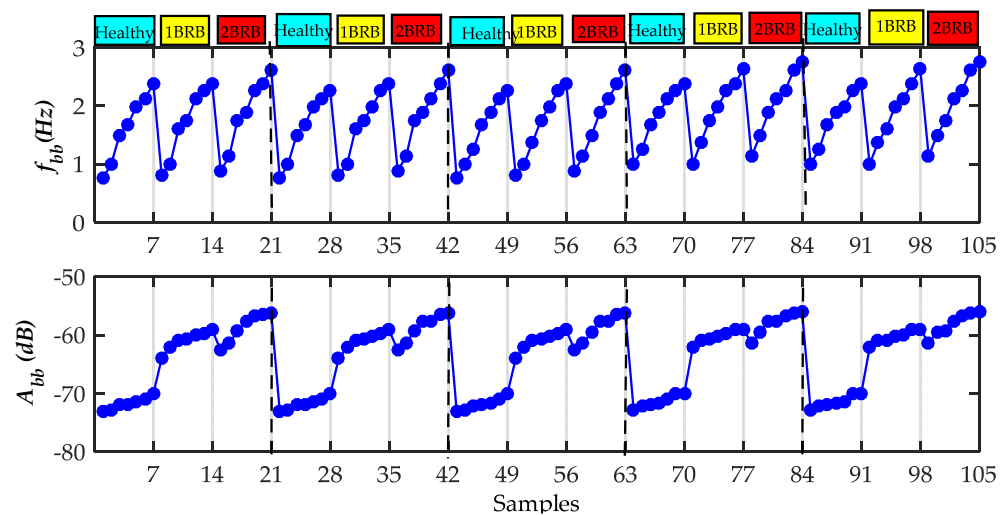

Figure 14. Inputs for the training data of the ANFIS models.

- 7×5 samples of a BRB fault with one broken bar under varying loads (10%, 20%, 40%, 50%, 70%, 80%, and 100%) of the rated load;
- 7×5 samples of a BRB fault with two broken bars under varying loads (10%, 20%, 40%, 50%, 70%, 80%, and 100%) of the rated load.

An output dataset is necessary to achieve supervised learning. This dataset was built by corresponding each sample in the input dataset with its desired output, which indicates the number of broken bars in the rotor of the IM for the two proposed models, as shown in Figure 15. It is clear that the ANFIS models perfectly learned the input dataset where they correctly gave the desired output with respect to the following scenarios:

- Output = 0, healthy rotor cage;
- Output = 1, one broken bar in the fault;
- Output = 2, two broken bars in the fault.

Figure 16 shows the training error of the ANFIS-GP and ANFIS-SC models in several conditions (healthy and faulty mode) of IMs. It is noted that the error values were very low in the two ANFIS models; comparing the responses of the proposed models, one can easily deduce that the ANFIS-SC model was stable, with minimal error compared to the ANFIS-GP model.
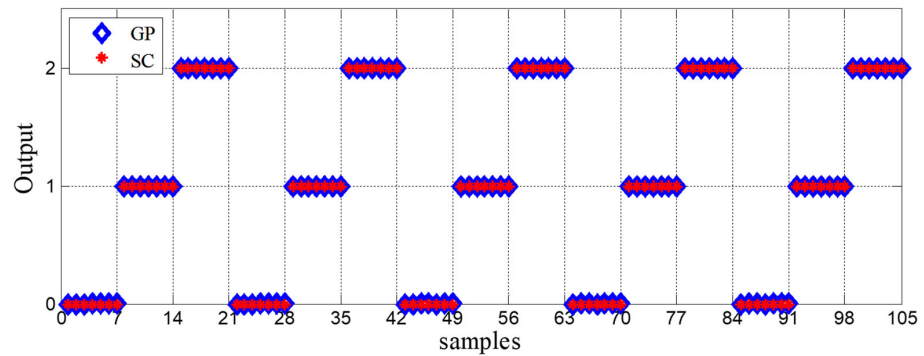
Figure 15. Output for the training data of the ANFIS models: ANFIS-GP and ANFIS-SC.
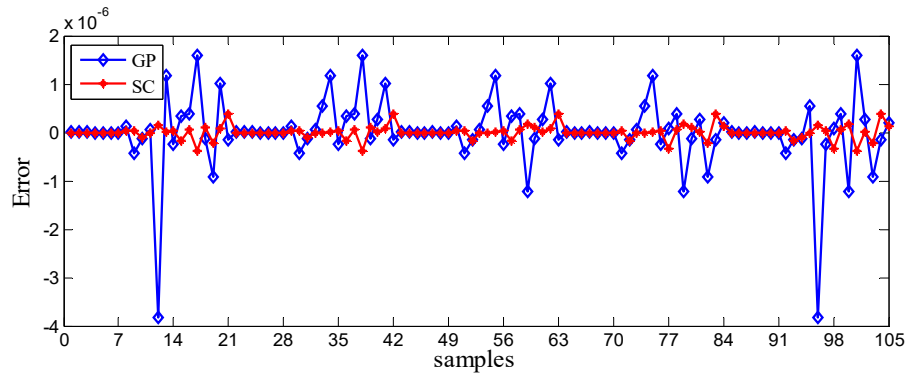

Figure 16. Errors of the ANFIS models' training data: ANFIS-GP and ANFIS-SC.

(b)   Test phase

In order to evaluate the two ANFIS models' ability to generalize with unknown data, the network must be tested with a testing subset. This is shown in Figure 17. Its distribution can be summarized as follows:

- Nine samples for healthy operating under varying loads (30%, 60%, and 90% of the rated load);
- Nine samples for the IM operating with one broken bar under varying loads (30%, 60%, and 90% of the rated load);
- Nine samples for the IM operating with two broken bars under varying loads (30%, 60%, and 90% of the rated load).
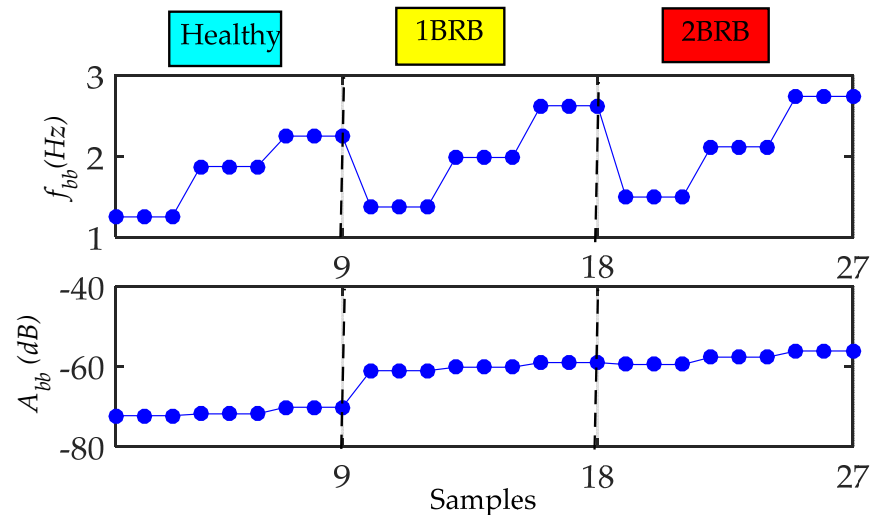

Figure 17. The inputs for the testing data of the ANFIS models.

The test outputs and their errors are shown in Figures 18 and 19, respectively, where it is noted that the network indicated variable outputs which represented the number of broken bars in the rotors of the IMs. The ANFIS-SC model can quantify the number of broken bars with higher accuracy and time effectiveness compared to the ANFIS-GP model.
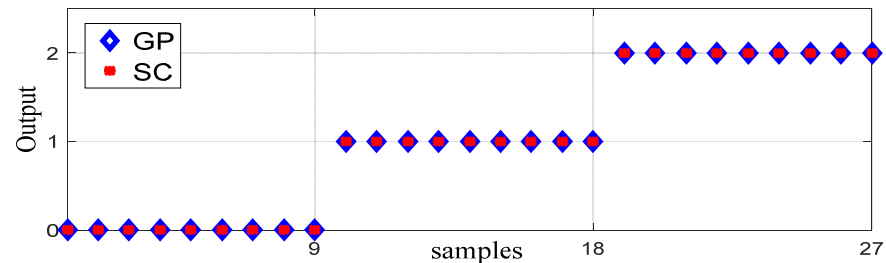

Figure 18. The output for the testing data of the ANFIS models: ANFIS-GP and ANFIS-SC.
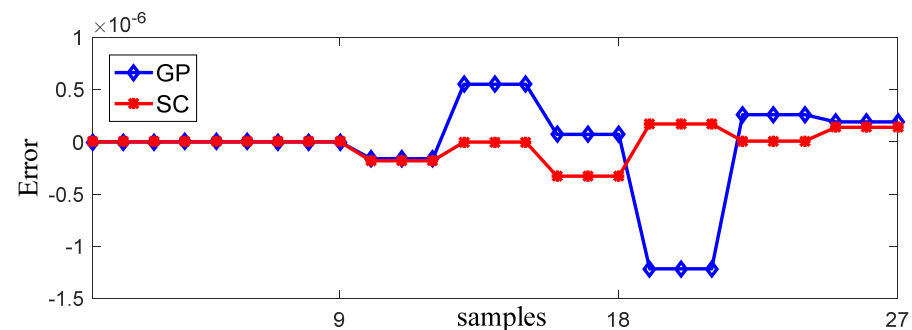

Figure 19. The error for the testing data of the ANFIS models: ANFIS-GP and ANFIS-SC.

(c)   Comparison between the two proposed ANFIS models

Table 3 represents the calculated performance criteria (MSE and RMSE) of the two ANFIS models for the learning and testing phases. From this table, it is observed that the ANFIS-SC model with (MSE = 1.9152×10^{-14}, and RMSE = 1.3839×10^{-7} for the training phase and MSE = 2.1088×10^{-14}, and RMSE = 1.4522×10^{-7} in the testing phase provided better results compared to ANFIS-GP. The high accuracy of ANFIS- SC can be explained by the nature of the algorithm since it groups data with similar information around a cluster center. The main advantage of this algorithm is that data points are used as candidates, which efficiently solves the dimensionality problems and reduces training time. Regarding the implementation purposes of the proposed algorithm, the cost is considerably reduced because of the reduction in ANFIS rules thanks to the optimized clusters. In addition, it is known that increasing the number of rules leads to stability problems because of the inference phenomenon, which is the key idea of all fuzzy systems.

The performance indices shown in Table 4 confirm the elevated performance and efficiency of the ANFIS-SC model, which can be successfully used for the detection and classification of BRB faults by determining the number of broken bars in the rotors of IMs. Furthermore, by comparing these results with those mentioned in the literature, it was observed that ANFIS models are one of the most effective algorithms in the literature in terms of CPU time and accuracy classification thanks to their high training ability, training time effectiveness, and software programming and hardware implementation cost compared to the other algorithms summarized in Table 5. However, in order to ensure the effectiveness of an ANFIS, one should consider input number reduction and its optimization since this determines the number of modifiable parameters.

Table 4. Comparison between the results of the two ANFIS models.

Phase	ANFIS Model	RMSE	MSE
Training	GP	7.3541×10^{-7}	5.4083×10^{-13}
	SC	$\mathbf{1.3839 \times 10^{-7}}$	$\mathbf{1.9152 \times 10^{-14}}$
Testing	GP	4.6240×10^{-7}	2.1381×10^{-13}
	SC	$\mathbf{1.4522 \times 10^{-7}}$	$\mathbf{2.1088 \times 10^{-14}}$

Table 5. Summary of selected papers with the aim of BRB detection.

Ref.	Input Data	Nature of Study	Signal Processing	Classifier Type	CPU Time	Advantages	Drawbacks
[27]	Current	E	SVMD	-	● ○ ○	- No need for training; - Efficient.	- Regression Curve efficiency.
[39]	Current + Vibration	E	FFT	ATSC-NEX	● ● ●	- Automatic construction; - High accuracy.	- Hyperparameter optimization.
[33]	Current	E	DWT	Fuzzy	● ● ○	- Simple configuration; - High accuracy.	- Optimization. of MFs and rules.
[38]	Current	T	FFT	Fuzzy	● ○ ○	- Simple configuration.	- No experimental validation; - Optimization of MFs and rules.
[50]	Current	E	DWTAR	ANFIS	● ● ○	- Simple configuration; - Efficient.	- No optimization procedures have been carried out.
[28]	Vibration	T + E	CMSA	-	● ● ●	- No need for training; - Efficient.	- Computational complexity.
[37]	Magnetic flux density	E	FFT	ANFISFUZZY	● ○ ○	- Simple configuration; - High accuracy.	- High number of inputs; - The use of six inputs.
[51]	Current	E	FFT	ANFIS	● ○ ○	- Simple configuration; - Efficient; - Cluster radius optimization; - Efficient.	- The maintained clusters lead to best result. However, the algorithm implementation becomes expensive because of the cluster number.
[36]	Current	T	WP	ANFIS	● ● ●	- Simple configuration; - High accuracy.	- The use of eight MFs for each input is not recommended for GP-ANFIS because of overfitting and the number of modifiable parameters, as reported in [49].
[22]	Current	T	HFFT	NN	● ● ●	- High accuracy.	- Important number of hidden layers and neurons in each one (time consumptions + overfitting).
[35]	Current	T	–	ANFIS	● ○ ○	- Simple configuration; - Efficient.	- Fault identification; - No test or validation.
[29]	Current	E	HFFT	Fuzzy	● ○ ○	- Simple configuration.	- Optimization of MFs and rules.
[34]	Current	T	DWT + PCA	ANFIS	● ● ●	- Simple configuration; - Efficient.	- The use of five parallel ANFIS models is computationally expensive.

E: Experimental; T: Theoretical; ● ○ ○ Low CPU time; ● ● ○ Medium CPU time; ● ● ● High CPU time.

6. Conclusions

The present paper proposes an effective diagnostic approach for the automatic early detection and classification of BRB faults in IMs under different loads. The approach is based on the hybridization of the HFFT method and two ANFIS models. The HFFT is applied by using the HT to extract the envelope of the stator current then processing it with FFT. The frequency and the amplitude of the $2sf_s$ spectrum of the stator current envelope were chosen as fault indicators, and they were used as the inputs of the ANFIS-GP and ANFIS-SC models. The proposed approach was implemented through experimental tests where three IMs were used: the first had one broken bar, the second had two adjacent broken bars, and the third was a healthy motor under different loads. The experimental results illustrated that:

- The amplitude (A_{bb}) and frequency (f_{bb}) of the *$2sf_s$* harmonic had a high sensibility of BRB faults, even under low loads (low slip), which allows them to be good and reliable indicators that easily detect BRB faults in IMs.
- Two ANFIS models, ANFIS-GP and ANFIS-SC networks, were used to classify the BRB faults by determining the number of broken bars in the rotors of IMs where it considered the A_{bb} and f_{bb} indicators as their inputs. The performance criteria, which represent the MSE and RMSE, show that the ANFIS-SC model provided the best detection and accuracy classification of the BRB faults, where a minimal error was obtained with MSE = 1.9152×10^{-14} and RMSE = 1.3839×10^{-7} in the training and about MSE = 2.1088×10^{-14} and RMSE = 1.4522×10^{-7} in the test comparison with the ANFIS-GP model.
- The combination of HFFT-ANFIS-SC provided the proposed approach with more effectiveness and accuracy for detecting the BRB faults and precisely quantifying the number of broken bars under different loads (under low and high slips).

The ANFIS networks, in particular "ANFIS-SC", did not fail in all cases of the scenarios. As a result, this diagnostic method may be used to detect other types of motor faults. As a consequence, as the scope of this study develops, the research can expand by considering other types of IM defects, such as eccentricity, bearings, inter-turn short circuits, etc., to obtain a reliable integrated automatic diagnostic system. Regarding future algorithmic development, an optimized bio-inspired ANFIS-SC could increase the machine learning capabilities of ANFIS. In addition, a deep encoder–decoder stacked ANFIS can make a considerable contribution to the BRB detection and deep learning field.

Author Contributions: Conceptualization, S.E.C. and H.C.; Data curation, H.C.; Formal analysis, S.E.C. and H.C.; Investigation, S.E.C. and H.C.; Methodology, H.C., S.E.C., M.I.M. and A.M.B.; Software, S.E.C.; Supervision, M.I.M., M.A. and A.M.B.; Validation, H.C.; Visualization, S.E.C.; Writing—original draft, H.C. and S.E.C.; Writing—review and editing, S.E.C., H.C., M.I.M., M.A. and A.M.B. All authors have read and agreed to the published version of the manuscript.

Data Availability Statement: Not applicable.

Conflicts of Interest: The authors declare no conflict of interest.

Abbreviations

BRB	Broken Rotor Bar
HT	Hilbert Transform
IM	Induction Motor
ANFIS	Adaptive Neuro-Fuzzy Inference System
GP	Grid Partitioning
SC	Subtractive Clustering
MCSA	Motor Current Signature Analysis

FFT	Fast Fourier Transform
HFFT	Hilbert Fast Fourier Transform
f_s	The Fundamental Harmonic
s	Rotor Slip

References

1. Lee, C.-Y. Effects of unbalanced voltage on the operation performance of a three-phase induction motor. *IEEE Trans. Energy Convers.* **1999**, *14*, 202–208.
2. Thorsen, O.V.; Dalva, M. Failure identification and analysis for high-voltage induction motors in the petrochemical industry. *IEEE Trans. Ind. Appl.* **1999**, *35*, 810–818. [CrossRef]
3. Craig, K.; Sinclair, A. Motor protection retrofit: A business case. In Proceedings of the 2011 64th Annual Conference for Protective Relay Engineers, College Station, TX, USA, 11–14 April 2011.
4. Ayhan, B.; Chow, M.-Y.; Song, M.-H. Multiple signature processing-based fault detection schemes for broken rotor bar in induction motors. *IEEE Trans. Energy Convers.* **2005**, *20*, 336–343. [CrossRef]
5. Zhang, P.; Du, Y.; Habetler, T.G.; Lu, B. A survey of condition monitoring and protection methods for medium-voltage induction motors. *IEEE Trans. Ind. Appl.* **2011**, *47*, 34–46. [CrossRef]
6. Liu, D.; Lu, D. Off-the-grid compressive sensing for broken-rotor-bar fault detection in squirrel-cage induction motors. *IFAC-PapersOnLine* **2015**, *48*, 1451–1456. [CrossRef]
7. Ameid, T.; Menacer, A.; Talhaoui, H.; Azzoug, Y. Discrete wavelet transform and energy eigen value for rotor bars fault detection in variable speed field-oriented control of induction motor drive. *ISA Trans.* **2018**, *79*, 217–231. [CrossRef] [PubMed]
8. Talhaoui, H.; Menacer, A.; Kessal, A.; Kechida, R. Fast Fourier and discrete wavelet transforms applied to sensorless vector control induction motor for rotor bar faults diagnosis. *ISA Trans.* **2014**, *53*, 1639–1649. [CrossRef]
9. Harzelli, I.; Menacer, A.; Ameid, T. A fault monitoring approach using model-based and neural network techniques applied to input–output feedback linearization control induction motor. *J. Ambient. Intell. Humaniz. Comput.* **2019**, *11*, 2519–2538. [CrossRef]
10. Hwang, D.H.; Youn, Y.W.; Sun, J.H.; Kim, Y.H. Robust diagnosis algorithm for identifying broken rotor bar faults in induction motors. *J. Electr. Eng. Technol.* **2014**, *9*, 37–44. [CrossRef]
11. Talhaoui, H.; Menacer, A.; Kessal, A.; Tarek, A. Experimental diagnosis of broken rotor bars fault in induction machine based on Hilbert and discrete wavelet transforms. *Int. J. Adv. Manuf. Technol.* **2018**, *95*, 1399–1408. [CrossRef]
12. Rangel-Magdaleno, J.; Peregrina-Barreto, H.; Ramirez-Cortes, J.; Cruz-Vega, I. Hilbert spectrum analysis of induction motors for the detection of incipient broken rotor bars. *Measurement* **2017**, *109*, 247–255. [CrossRef]
13. Kechida, R.; Menacer, A.; Talhaoui, H. Approach signal for rotor fault detection in induction motors. *J. Fail. Anal. Prev.* **2013**, *13*, 346–352. [CrossRef]
14. Aydin, I.; Karakose, M.; Akin, E. A new method for early fault detection and diagnosis of broken rotor bars. *Energy Convers. Manag.* **2011**, *52*, 1790–1799. [CrossRef]
15. Morinigo-Sotelo, D.; Romero-Troncoso, R.D.J.; Panagiotou, P.A.; Antonino-Daviu, J.A.; Gyftakis, K.N. Reliable detection of rotor bars breakage in induction motors via MUSIC and ZSC. *IEEE Trans. Ind. Appl.* **2017**, *54*, 1224–1234. [CrossRef]
16. Martin-Diaz, I.; Morinigo-Sotelo, D.; Duque-Perez, O.; Arredondo-Delgado, P.A.; Camarena-Martinez, D.; Romero-Troncoso, R.J. Analysis of various inverters feeding induction motors with incipient rotor fault using high-resolution spectral analysis. *Electr. Power Syst. Res.* **2017**, *152*, 18–26. [CrossRef]
17. Singh, G.; Naikan, V. Detection of half broken rotor bar fault in VFD driven induction motor drive using motor square current MUSIC analysis. *Mech. Syst. Signal Process.* **2018**, *110*, 333–348. [CrossRef]
18. Karmakar, S.; Chattopadhyay, S.; Mitra, M.; Sengupta, S. *Induction Motor Fault Diagnosis*; Springer: Berlin/Heidelberg, Germany, 2016; Volume 25.
19. Sharma, A.; Mathew, L.; Chatterji, S.; Goyal, D. Artificial Intelligence-Based Fault Diagnosis for Condition Monitoring of Electric Motors. *Int. J. Pattern Recognit. Artif. Intell.* **2019**, *34*, 2059043. [CrossRef]
20. Goyal, D.; Dhami, S.; Pabla, B. Non-Contact Fault Diagnosis of Bearings in Machine Learning Environment. *IEEE Sens. J.* **2020**, *20*, 4816–4823. [CrossRef]
21. Glowacz, A.; Glowacz, W.; Glowacz, Z.; Kozik, J. Early fault diagnosis of bearing and stator faults of the single-phase induction motor using acoustic signals. *Measurement* **2018**, *113*, 1–9. [CrossRef]
22. Bessam, B.; Menacer, A.; Boumehraz, M.; Cherif, H. Detection of broken rotor bar faults in induction motor at low load using neural network. *ISA Trans.* **2016**, *64*, 241–246. [CrossRef]
23. Khechekhouche, A.; Cherif, H.; Benakcha, A.; Menacer, A.; Chehaidia, S.E.; Panchal, H. Experimental diagnosis of inter-turns stator fault and unbalanced voltage supply in induction motor using MCSA and DWER. *Period. Eng. Nat. Sci.* **2020**, *8*, 1202–1216.
24. Cherif, H.; Benakcha, A.; Laib, I.; Chehaidia, S.E.; Menacer, A.; Soudan, B.; Olabi, A.G. Early detection and localization of stator inter-turn faults based on discrete wavelet energy ratio and neural networks in induction motor. *Energy* **2020**, *212*, 118684. [CrossRef]
25. Talhaoui, H.; Ameid, T.; Kessal, A. Energy eigenvalues and neural network analysis for broken bars fault diagnosis in induction machine under variable load: Experimental study. *J. Ambient. Intell. Humaniz. Comput.* **2021**, *13*, 2651–2665. [CrossRef]

26. Liu, R.; Yang, B.; Zio, E.; Chen, X. Artificial intelligence for fault diagnosis of rotating machinery: A review. *Mech. Syst. Signal Process.* **2018**, *108*, 33–47. [CrossRef]

27. Liu, X.; Yan, Y.; Hu, K.; Zhang, S.; Li, H.; Zhang, Z.; Shi, T. Fault Diagnosis of Rotor Broken Bar in Induction Motor Based on Successive Variational Mode Decomposition. *Energies* **2022**, *15*, 1196. [CrossRef]

28. Wang, Z.; Yang, J.; Li, H.; Zhen, D.; Xu, Y.; Gu, F. Fault identification of broken rotor bars in induction motors using an improved cyclic modulation spectral analysis. *Energies* **2019**, *12*, 3279. [CrossRef]

29. Laala, W.; Zouzou, S.-E.; Guedidi, S. Induction motor broken rotor bars detection using fuzzy logic: Experimental research. *Int. J. Syst. Assur. Eng. Manag.* **2014**, *5*, 329–336. [CrossRef]

30. Gyftakis, K.N.; Cardoso, A.J.M.; Antonino-Daviu, J.A. Introducing the Filtered Park's and Filtered Extended Park's Vector Approach to detect broken rotor bars in induction motors independently from the rotor slots number. *Mech. Syst. Signal Process.* **2017**, *93*, 30–50. [CrossRef]

31. Halder, S.; Bhat, S.; Dora, B.K. Inverse thresholding to spectrogram for the detection of broken rotor bar in induction motor. *Measurement* **2022**, *198*, 111400. [CrossRef]

32. Stief, A.; Baranowski, J. Fault diagnosis using Interpolated Kernel Density Estimate. *Measurement* **2021**, *176*, 109230. [CrossRef]

33. Sabir, H.; Ouassaid, M.; Ngote, N. An experimental method for diagnostic of incipient broken rotor bar fault in induction machines. *Heliyon* **2022**, *8*, e09136. [CrossRef] [PubMed]

34. Juneghani, M.A.; Boroujeni, B.K.; Abdollahi, M. Determination of number of broken rotor bars in squirrel-cage induction motors using adaptive neuro-fuzzy interface system. *Res. J. Appl. Sci. Eng. Technol.* **2012**, *4*, 3399–3405.

35. Sayed, M.A.M.M.A.; Hassan, E.A.M.M. Detection and classification of broken rotor bars faults in induction motor using adaptive neuro-fuzzy inference system. In Proceedings of the MEPCON '14, Cairo, Egypt, 23–25 December 2014.

36. Merabet, H.; Bahi, T.; Drici, D.; Halam, N.; Bedoud, K. Diagnosis of rotor fault using neuro-fuzzy inference system. *J. Fundam. Appl. Sci.* **2017**, *9*, 170–182. [CrossRef]

37. Dias, C.G.; de Sousa, C.M. A neuro-fuzzy approach for locating broken rotor bars in induction motors at very low slip. *J. Control Autom. Electr. Syst.* **2018**, *29*, 489–499. [CrossRef]

38. Chouidira, I.; Khodja, D.E.; Chakroune, S. Fuzzy logic based broken bar fault diagnosis and behavior study of induction machine. *J. Eur. Syst. Autom.* **2021**, *53*, 233–242. [CrossRef]

39. Tahkola, M.; Szücs, Á.; Halme, J.; Zeb, A.; Keränen, J. A Novel Machine Learning-Based Approach for Induction Machine Fault Classifier Development—A Broken Rotor Bar Case Study. *Energies* **2022**, *15*, 3317. [CrossRef]

40. Islam, M.M.; Kim, J.-M. Time–frequency envelope analysis-based sub-band selection and probabilistic support vector machines for multi-fault diagnosis of low-speed bearings. *J. Ambient. Intell. Humaniz. Comput.* **2017**, 1–16. [CrossRef]

41. Yang, B.-S.; Oh, M.-S.; Tan, A.C.C. Fault diagnosis of induction motor based on decision trees and adaptive neuro-fuzzy inference. *Expert Syst. Appl.* **2009**, *36*, 1840–1849.

42. Puche-Panadero, R.; Pineda-Sanchez, M.; Riera-Guasp, M.; Roger-Folch, J.; Hurtado-Perez, E.; Perez-Cruz, J. Improved resolution of the MCSA method via Hilbert transform, enabling the diagnosis of rotor asymmetries at very low slip. *IEEE Trans. Energy Convers.* **2009**, *24*, 52–59. [CrossRef]

43. Jang, J.-S. ANFIS: Adaptive-network-based fuzzy inference system. *IEEE Trans. Syst. Man Cybern.* **1993**, *23*, 665–685. [CrossRef]

44. Parey, A.; Singh, A. Gearbox fault diagnosis using acoustic signals, continuous wavelet transform and adaptive neuro-fuzzy inference system. *Appl. Acoust.* **2019**, *147*, 133–140. [CrossRef]

45. Chehaidia, S.E.; Abderezzak, A.; Kherfane, H.; Boukhezzar, B.; Cherif, H. An improved machine learning techniques fusion algorithm for controls advanced research turbine (Cart) power coefficient estimation. *UPB Sci. Bull. Ser. C Electr. Eng. Comput. Sci.* **2020**, *82*, 279–292.

46. Cheng, F.; Qu, L.; Qiao, W. Fault Prognosis and Remaining Useful Life Prediction of Wind Turbine Gearboxes Using Current Signal Analysis. *IEEE Trans. Sustain. Energy* **2018**, *9*, 157–167. [CrossRef]

47. Fattahi, H. Indirect estimation of deformation modulus of an in situ rock mass: An ANFIS model based on grid partitioning, fuzzy c-means clustering and subtractive clustering. *Geosci. J.* **2016**, *20*, 681–690. [CrossRef]

48. Fattahi, H.; Bayatzadehfard, Z. A comparison of performance of several artificial intelligence methods for estimation of required rotational torque to operate horizontal directional drilling. *Iran Univ. Sci. Technol.* **2017**, *7*, 45–70.

49. Asghar, A.B.; Liu, X. Estimation of wind turbine power coefficient by adaptive neuro-fuzzy methodology. *Neurocomputing* **2017**, *238*, 227–233. [CrossRef]

50. Mohamed, M.A.; Hassan, M.A.M.; Albalawi, F.; Ghoneim, S.S.; Ali, Z.M.; Dardeer, M. Diagnostic Modelling for Induction Motor Faults via ANFIS Algorithm and DWT-Based Feature Extraction. *Appl. Sci.* **2021**, *113*, 9115. [CrossRef]

51. Karnavas, Y.L.; Chasiotis, I.D.; Vrangas, A. Fault diagnosis of squirrel-cage induction motor broken bars based on a model identification method with subtractive clustering. In Proceedings of the 2017 IEEE 11th International Symposium on Diagnostics for Electrical Machines, Power Electronics and Drives (SDEMPED), Tinos, Greece, 29 August–1 September 2017.